Environmental Science and Pollution Research (2022) 29:51703–51716
https://doi.org/10.1007/s11356-022-19460-z

RESEARCH ARTICLE

Capability of copper–nickel ferrite nanoparticles loaded onto multi-walled carbon nanotubes to degrade acid blue 113 dye in the sonophotocatalytic treatment process

Tariq J. Al-Musawi[1] · Nezamaddin Mengelizadeh[2] · Mahmoud Taghavi[3] · Zaccheus Shehu[4] · Davoud Balarak[5]

Received: 18 June 2021 / Accepted: 23 February 2022 / Published online: 5 March 2022

Abstract

In this study, copper–nickel ferrite ($CuNiFe_2O_4$) nanoparticles were successfully loaded onto multi-walled carbon nanotubes (MWCNTs) by using the coprecipitation method and used as new catalysts (MWCNT–$CuNiFe_2O_4$) in the sonophotocatalytic degradation process of the acid blue 113 (AB113) dye. The success of the MWCNT–$CuNiFe_2O_4$ synthesis and its properties were determined by analyzing it using field emission scanning electron microscopy (FESEM), transmission electron microscopy (TEM), X-ray powder diffraction (XRD), and Fourier transform infrared spectroscopy (FTIR). A high efficiency of dye removal (100%), total organic carbon (93%), and chemical oxygen demand (95%) were achieved with the following conditions: pH of dye solution = 5, MWCNT–$CuNiFe_2O_4$ dosage = 0.6 g/L, AB113 dye concentration = 50 mg/L, UV light intensity = 36 W, ultrasonic wave frequency = 35 kHz, and treatment time = 30 min. The kinetic results revealed that the efficiency of the sonophotocatalytic process using MWCNT–$CuNiFe_2O_4$ was higher than that of the sonolysis, photolysis, photocatalysis, and sonocatalysis processes. Scavenging studies demonstrated that the holes (h^+) and hydroxyl radical (•OH) were the main reactive species for the AB113 dye degradation. The stability and recyclability of MWCNT–$CuNiFe_2O_4$ were confirmed with eight consecutive cycles for a maximum efficiency of more than 92%. The high rate of BOD_5/COD indicated that the sonophotocatalytic process had the potential to degrade the dye into degradable compounds. The toxicity study with an *Escherichia coli* growth inhibition rate emphasized that MWCNT–$CuNiFe_2O_4$ in the sonophotocatalytic degradation process of the AB113 dye had a significant effect on reducing toxicity, when compared to processes of photolysis and photocatalysis. During the sonophotocatalytic process using MWCNT–$CuNiFe_2O_4$, the AB113 dye was mineralized into CO_2, H_2O, NH_4^+, NO_3^-, and SO_4^{2-}. The results of the present study proved that the MWCNT–$CuNiFe_2O_4$-based sonophotocatalytic process was a promising dye degradation technology to protect the aquatic environment.

Keywords MWCNT–$CuNiFe_2O_4$ · Sonophotocatalytic · Acid blue 113 · Toxicity · Mineralization · Degradation efficiency

Introduction

In recent times, one of the concerns of environmentalists has been the pollution of water resources by sewage discharged from various industries, especially textile industries (Muhambihai et al., 2020). Today, more than ten thousand types of dyes are produced at an annual rate of 0.6×10^6, of which approximately 10% are discharged as waste, eventually getting into the environment via pumped dye wastewater. The introduction of dye wastewater into the aquatic system will increase the level of toxic compounds, chemical oxygen demand (COD), and the suspended solids (Samarghandi et al. 2020). The acid blue 113

Responsible Editor: Sami Rtimi.

✉ Davoud Balarak
dbalarak2@gmail.com

[1] Building and Construction Techniques Engineering Department, Al-Mustaqbal University College, Babylon, Iraq

[2] Department of Environmental Health Engineering, Evas Faculty of Health, Larestan University of Medical Sciences, Larestan, Iran

[3] Department of Environmental Health Engineering, Social Determinants of Health Research Center, Gonabad University of Medical Sciences, Gonabad, Iran

[4] Department of Chemistry, Faculty of Science, Gombe State University, Gombe, Nigeria

[5] Department of Environmental Health, Health Promotion Research Center, Zahedan University of Medical Sciences, Zahedan, Iran

(AB113) dye is one of the common azo dyes used in the wool, polyamide, and plastic industries due to its properties of good adhesion and high stability (Samarghandi et al. 2020; Asghar et al. 2019). The International Agency for Research on Cancer categorized the AB113 dye to be a hazardous and carcinogenic agent for humans because of its aromatic rings and other toxic properties (Bolong et al. 2009). Therefore, dyes and their derivatives must be removed from the wastewater before discharging it into the environment. Generally, various techniques such as adsorption, coagulation, membranes, electro-oxidation, and chemical oxidation have been used to remove the organic pollutants (Samarghandi et al. 2020). Although various methods with advantages and disadvantages have been used to remove the contaminants, the photocatalytic process has received more attention recently due to features, such as its excellent mineralization, it being cost-effective, and its simple operation to degrade the dye into non-toxic and harmless materials (Samarghandi et al. 2020). Photocatalysis with titanium dioxide (TiO_2) is proposed as the most common, advanced technology for the efficient elimination of organic pollutants. However, the actual scale application of TiO_2 has not shown a good performance in the treatment of contaminated water, due to the rapid electron/hole (e^-/h^+) recombination (Hanh et al. 2020). To overcome this problem, researchers proposed different semiconductor photocatalysts, such as ZnO, SnO_2, Co_3O_4, Mn_3O_4, Cu_2S, and ZnS (Muhambihai et al. 2020). According to the findings of previous studies, such common semiconductor materials found that the photo-corrosion effect appeared after prolonged illumination, which reduced the photocatalytic stability of the materials and their recyclability (Muhambihai et al. 2020; Liu et al. 2020).

Compared to the semiconductor photocatalysts mentioned above, nanocomposites, which are composed of two different transition metals, have attracted more attention from researchers due to their excellent photocatalytic life and nano-heterojunction formation. Among catalysts, the MFe_2O_4 nanoparticles (M=Cu, Ni, Co, Zn), with magnetic and electronic properties, showed a photocatalytic potential for degrading pollutants (Sayadi et al. 2021; Ji et al. 2015; Amiri et al. 2019). Of late, researchers have proposed mixed ferrites as catalysts in environmental engineering applications because of their good energy gap, high level of chemical stability, and excellent ferroelectric-magnetic properties. In mixed ferrites, the presence of metals significantly increases the spinal ferrites and corrective properties for the degradation of target pollutants (Manohar et al. 2021; Soltani et al. 2013). Chahar et al. examined the catalytic activity of Co-$XnFe_2O_4$ for the degrading methylene blue dye and found high pollutant-removal efficiencies for the low weight percentage of transition metals substituted in mixed ferrites (Chahar et al. 2021). Meena et al. synthesized the Ce-doped $MnFe_2O_4$ nanomagnetic ferrites; they observed that the Ce-$MnFe_2O_4$ composite showed good results for dye degradation, due to the advantages of excellent mechanical–chemical stability and magnetic properties (Meena et al. 2021). Dojcinovic et al. synthesized mixed Mg-$CoFe_2O_4$ for photocatalytic degradation of the dye (Dojcinovic et al. 2021). Despite these advantages, mixed ferrite nanoparticles with magnetic properties easily aggregate and, therefore, have a negative impact on the degradation efficiency. To overcome such disadvantages, researchers proposed loading particles onto a supporting material such as graphene oxide and chitosan (Rahman et al. 2020; Nawaz et al. 2020; Shabbir et al. 2019). Among them, multi-walled carbon nanotubes (MWCNTs) have been considered as supporting materials, because of their high electrical conductivity, large surface area, and excellent adsorptive properties (Murali et al. 2020; Natarajan et al. 2020). Sun et al. reported that MWCNTs with good electrical properties and dispersion can be easily combined with semiconductors to induce charge transfer for improvement of catalytic activity (Sun et al. 2020). Tan et al. reported that MWCNTs, with a special functional group, could produce a synergistic effect with a semiconductor, to reduce the recombination rate of e^- and h^+. Moreover, MWCNTs alone, as an electron transporter, can extend the life and performance of the photocatalysts. On the other hand, this carbonic material with a porous and hollow structure can increase the interaction of polluting molecules with the loaded catalyst (Tan et al. 2020).

It has been reported that the degradation and mineralization performance of oxidation systems significantly improve when the process is used as a synergistic effect to activate oxidants. In recent years, the ultrasound (US) process has been combined with photocatalytic systems to improve mineralization at low reaction times (Cheng et al. 2012; Schieppati et al. 2019). When ultrasonic waves are applied to a liquid, the cavitation bubbles split the water molecules, which result in it producing •OH. At the same time, the ultrasonic waves also scatter the photocatalyst particles in the solution, which intensifies the treatment of the polluted solution (Schieppati et al. 2019). Babu et al. combined ultrasound (US) and CuO-TiO_2/rGO (as a photocatalyst) to degrade methylene orange dye and found a strong synergistic effect (3.7-fold) of US and photocatalysis (Babu et al. 2019). In addition, Babu et al. studied and compared the degradation efficiency of $LaFeO_3$ and Fe^{3+}/persulfate in the Fenton-like treatment system for several organic pollutants (Babu et al. 2017). To the knowledge of the researchers, studies on the degradation of organic pollutants by a MWCNT–$CuNiFe_2O_4$-based sonophotocatalytic process have not yet been made or reported.

Here, the researchers evaluated the combination of US with the photocatalytic process to degrade the AB113 dye. In this study, a new and novel photocatalyst was formed from loading $CuNiFe_2O_4$ nanoparticles onto MWCNTs (MWCNTs–$CuNiFe_2O_4$) and then synthesized. First, the surface and structural properties were determined by using advanced characterization analyses. Then, the effect of the operating factors on the dye degradation efficiency was investigated in detail. The concentrations of the SO_4^{2-}, NH_4^+, and NO_3^- ions formed at the end of the sonophotocatalytic process were detected. The toxicity of the treated AB113 dye

solution was evaluated by counting the *Escherichia coli* (*E. coli*) bacteria. Moreover, mineralization, catalyst reusability, and the mechanism of the AB113 dye degradation in the sonophotocatalytic reactions were all investigated.

Materials and methods

Chemicals

MWCNTs (purity > 95%, inside diameter = 5–10 nm, outside diameter = 20–30 nm, and length = 10–30 um) were provided by the Iranian Nanomaterials Pioneers Company (Tehran, Iran). $Cu(NO_3)_2.3H_2O$, $Fe(NO_3)_2.6H_2O$, $Ni(NO_3)_2.6H_2O$, NaOH, and H_2SO_4 were purchased from Merck (Germany). Ethylenediaminetetraacetic acid (EDTA), isopropyl alcohol (IPA), and 1,4-benzoquinone (BQ) were provided from Sigma Aldrich (USA). The AB113 dye ($C_{32}H_{21}N_5Na_2O_6S_2$, dye content = 50%) was used as a target contaminant and purchased from Sigma Aldrich (Germany). In addition, deionized water was used to prepare and dilute the working solutions.

MWCNT–$CuNiFe_2O_4$ synthesis

MWCNTs–$CuNiFe_2O_4$ was synthesized using the coprecipitation method, based on the methodology documented in the Al-Musawi et al. study (Al-Musawi et al. 2021a, b) (Fig. 1).

Sonophotocatalytic experiments

To conduct sonophotocatalytic experiments, a cylindrical Pyrex vessel (capacity = 250 mL) with a quartz plate on one side was employed as a reactor. An ultrasound bath (sunshine, SS-6508 T) was used for performing the US waves, where this device was operated at a supply power intensity of about 1–2 W/cm^{-2}. In addition, a UV light irradiation was performed via a mercury lamp (Philips, Netherlands). To begin with, a certain amount of the prepared MWCNTs–$CuNiFe_2O_4$ was added to 100 mL of AB113 dye solution (at the pre-determined concentration) and mixed at 180 rpm for 30 min under US and UV irradiation. During the mixing process, 1 mL of dye solution sample was withdrawn at various times, and the amount of dye absorption was determined via the absorption measurement. The UV–Vis absorption measurement of the AB113 dye concentration in aqueous solutions was performed by UV–Vis spectrophotometry (Unico 2100) at λ_{max} = 560 nm. The spectrophotometry readings were repeated thrice for each sample, and the mean removal efficiency was reported. During the experiment, the effect of the MWCNT–$CuNiFe_2O_4$ dosage (0.1–0.6 g/L), initial pH (3–11), UV light intensity (8–36 W), US frequency (20, 35, and 50 kHz), and initial concentration of the AB113 dye (10–100 mg/L) on the sonophotocatalytic degradation efficiency was investigated, by keeping the other parameters constant. The degradation efficiency of the AB113 dye was assessed by Eq. (1), as given (Al-Jubouri et al. 2021; Alhassani et al. 2020).

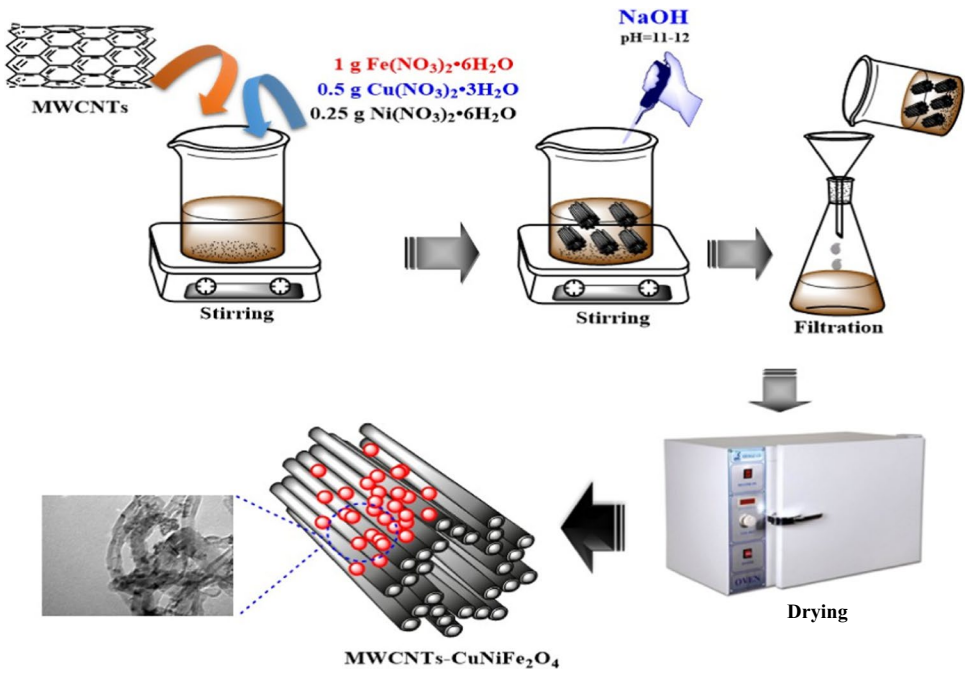

Fig. 1 Experimental steps used to synthesize MWCNT–$CuNiFe_2O_4$ catalyst

$$\text{Efficiency}\ (\%) = \frac{(C_0 - C_e)}{C_0} \times 100 \quad (1)$$

where C_0 and C_e represented the initial and final AB113 dye concentrations, respectively.

To investigate the present process and understand the removal mechanisms, comparison experiments between adsorption, sonolysis, photolysis, photocatalysis, and sonocatalysis systems on dye removal were done under an initial pH of 5, MWCNT–$CuNiFe_2O_4$ dosage of 0.6 g/L, UV light intensity of 36 W, US wave frequency of 35 kHz, and dye concentration of 50 mg/L. MWCNT–$CuNiFe_2O_4$ catalytic stability tests in AB113 degradation were evaluated for eight consecutive cycles. After each cycle, the used MWCNTs–$CuNiFe_2O_4$ was collected via filtration and centrifugation techniques and then washed with deionized water and ethanol (assay > 99%) to remove the residue. After being dried in a vacuum oven at 60 °C, the MWCNTs–$CuNiFe_2O_4$ was used for the next cycle in previous laboratory conditions. Scavenging experiments were performed to monitor reactive species involved in AB113 degradation. In this capturing test, 2 mM IPA, EDTA, and BQ were used as scavengers of •OH, h^+, and $•O_2^-$, respectively.

Toxicity test

E. coli was used to evaluate the toxicity of the treated solution. A number of test tubes containing broth lactate were sterilized in an autoclave. At the same time, the *E. coli* was incubated in an EMB agar medium at 37 °C for 24 h. To begin the toxicity test, a number of tubes were used as a control test and a number of others as a toxicity test, in the optimal condition (10 mL of culture medium + 1-mL reactor outlet + one microbe loop). After incubation at 37 °C, absorbance of the test tubes was performed at $\lambda = 600$ nm by UV–Vis spectrophotometry.

Characterization analyses and analytical methods

The crystalline structure of the MWCNTs–$CuNiFe_2O_4$ was determined by using an X-ray diffractometer (model: PW1730, Philips) with Cu Kα radiation, in the 10–80° range. Surface morphology and sample size were provided by scanning electron microscopy (SEM, MIRA III model, TESCAN, Czech) and transmission electron microscopy (TEM, CM120 model, Netherlands). Photocatalyst functional groups were recorded on a Fourier transform infrared spectroscopy (FTIR) device (AVATAR model, Thermo Co., USA) in a 400–4000-cm^{-1} wave number range. The analysis of BET was used to assess the specific surface area of the catalyst sample. The point of zero charge of the MWCNTs–$CuNiFe_2O_4$ was determined, based on the pH change in the NaCl solution containing the catalyst (Al-Musawi et al. 2021a, b).

Determination of the chemical oxygen demand (COD), 5-day biochemical oxygen demand (BOD_5), sulfate (SO_4^{2-}), ammonium (NH_4^+), and nitrate (NO_3^-) concentrations were performed according to the standard method (Federation et al. 2005). To determine the mineralization rate, the total organic carbon (TOC) analyzer (model: TOC-L, Shimadzu, Japan) was employed for the measurement of the TOC concentrations for the AB113 dye samples taken.

Results and discussion

Characterizations of MWCNTS–$CuNiFe_2O_4$

Morphological evaluation performed by the SEM image (Fig. 2a) shows that $CuNiFe_2O_4$ particles are loaded on the MWCNT surface, with a relatively uniform distribution. Moreover, in the TEM image (Fig. 2b), it can be seen that

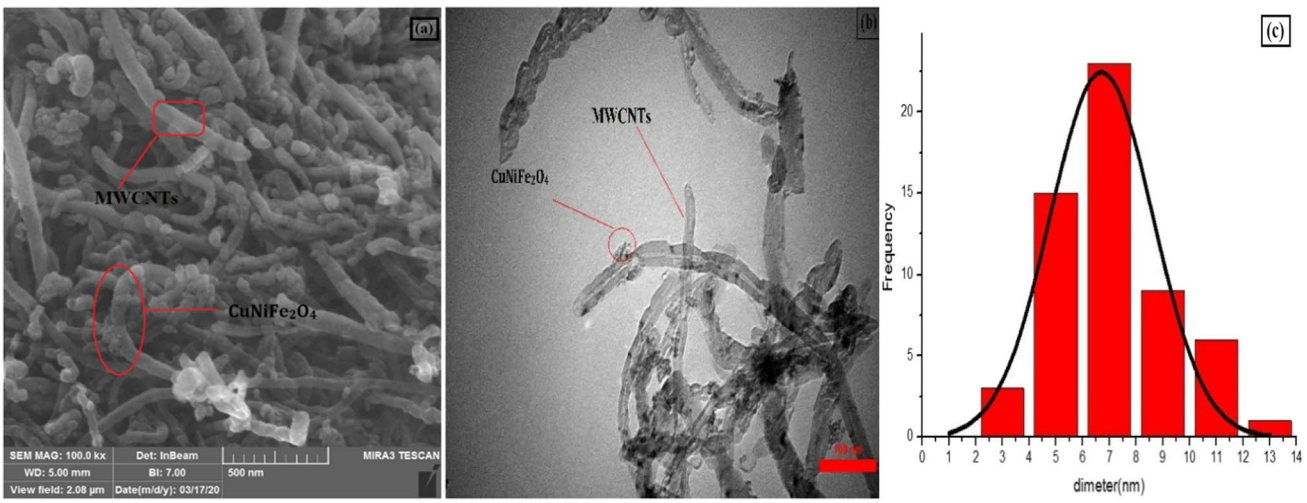

Fig. 2 SEM image (**a**), TEM image (**b**), and size distribution histogram (**c**) of MWCNTs–$CuNiFe_2O_4$

the $CuNiFe_2O_4$ particles are scattered on the outer wall of the MWCNTs. Figure 2c shows a diameter distribution histogram based on the TEM image. According to this figure, the average diameter was between of 3 and 14 nm.

Figure 3a shows the XRD patterns of MWCNTs and MWCNTs–$CuNiFe_2O_4$. It can be noted that the XRD pattern of MWCNTs has two characteristic peaks around 25° and 42°, which correspond to (002) and (100) planes (Tan et al. 2020). On the other hand, the MWCNTs–$CNiFe_2O_4$ has characteristic peaks around 16.96°, 32.5°, 46.29°, 57.21, and 66.89°, which relate to planes (111), (220), (400), (440), and (511) (Rao et al. 2016; Rajabzadeh et al. 2018). In fact, the disappearance of the two XRD peaks of MWCNTs in MWCNTs–$CNiFe_2O_4$ can be attributed to the degradation process of these materials when the $CuNiFe_2O_4$ is loading onto MWCNTs. The FTIR spectra of the MWCNTs and MWCNTs–$CuNiFe_2O_4$ are shown in Fig. 3b. Clearly, this figure reveals a peak of ferrites that are observed between 500 and 600 cm^{-1} wave number, which result from the stretching vibration of Fe–O at the tetrahedral sites (Soomro et al. 2017). In addition, the sharp peaks observed at wave numbers of 1120, 1380, 1600, and 3440 cm^{-1} are related to C–OH bending, N–H bending, and O–H stretching vibrations, respectively (Moazzen et al. 2019; Yaghoubi et al. 2018). Similar results were noted by Zhang et al. (Zhang et al. 2016); Mujahid et al. (Mujahid et al. 2019); and Hezam et al. (Hezam et al. 2020) for ferrites loaded on MWCNTs. In addition, according to the BET analysis, the MWCNTs–$CuNiFe_2O_4$ has a high surface area (121.09 m^2/g) which is considered as a favorable parameter that can improve the performance of the photocatalytic properties of this catalyst.

Effect of operating factors

Adsorption behavior and surface charge characteristics of the photocatalyst and the contaminant can be altered by changing the pH of the solution. Therefore, in the current study, the effect of pH (3–11) on the degradation efficiency of the AB113 dye is evaluated; the results are shown in Fig. 4a. The condition of this experiment has been fixed at MWCNT–$CuNiFe_2O_4$ dosage = 0.6 g/L, dye concentration = 50 mg/L, ultrasound frequency = 35 kHz, and UV intensity = 36 W. As noted, the degradation efficiency of the dye decreases from 100 to 54.11%, by increasing the solution pH from 3 to 11. These changes can be explained in accordance with changes in the surface charge of the pollutant and the photocatalyst. The point of zero charge obtained for MWCNTs–$CuNiFe_2O_4$ is 7.8. Thus, the particle surface is positive at pH < 7.8, and the charge is negative at pH > 7.8. On the other hand, AB113 has two sulfonate ($-SO_3^-$) groups with a pKa of 0.5 (Mortazavian et al. 2019). Due to that, the dye has a tendency to have a negative charge at pH > 0.5. Based on these properties, strong adsorption at an acidic pH can occur between dye molecules and MWCNT–$CuNiFe_2O_4$ functional groups. However, the repulsive electrostatic interactions between the anionic dyes and negative surface of the photocatalysts can be developed in alkaline conditions. Moreover, the presence of high amounts of the hydroxyl ion (OH^-) at an alkaline pH will prevent the adsorption of anionic dye molecules onto the photocatalyst. Similar results have been obtained by He et al. for the photocatalytic degradation of methylene orange and its products (He et al. 2011).

The effect of adding different amounts of a photocatalyst on the photodegradation efficiency of the dye is presented

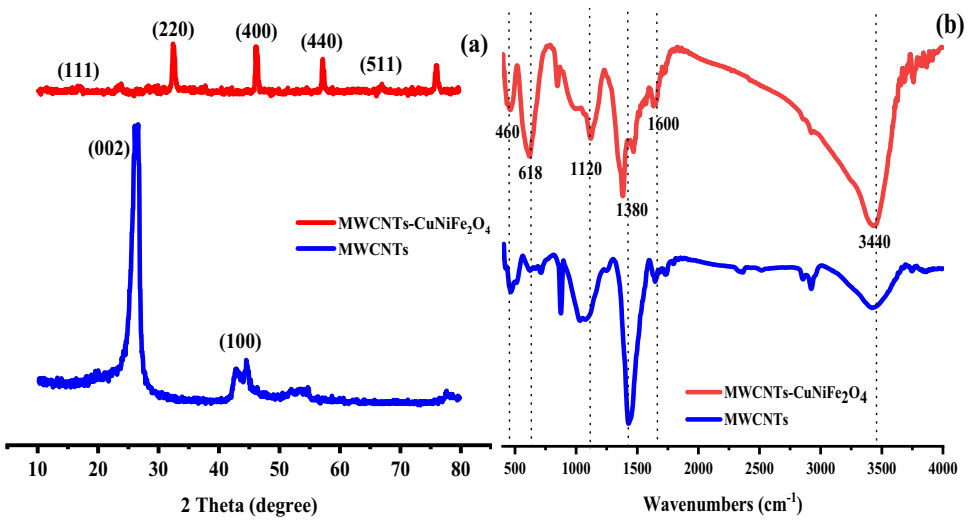

Fig. 3 XRD pattern (**a**) and FTIR spectra (**a**) of MWCNTs and MWCNTs–$CuNiFe_2O_4$

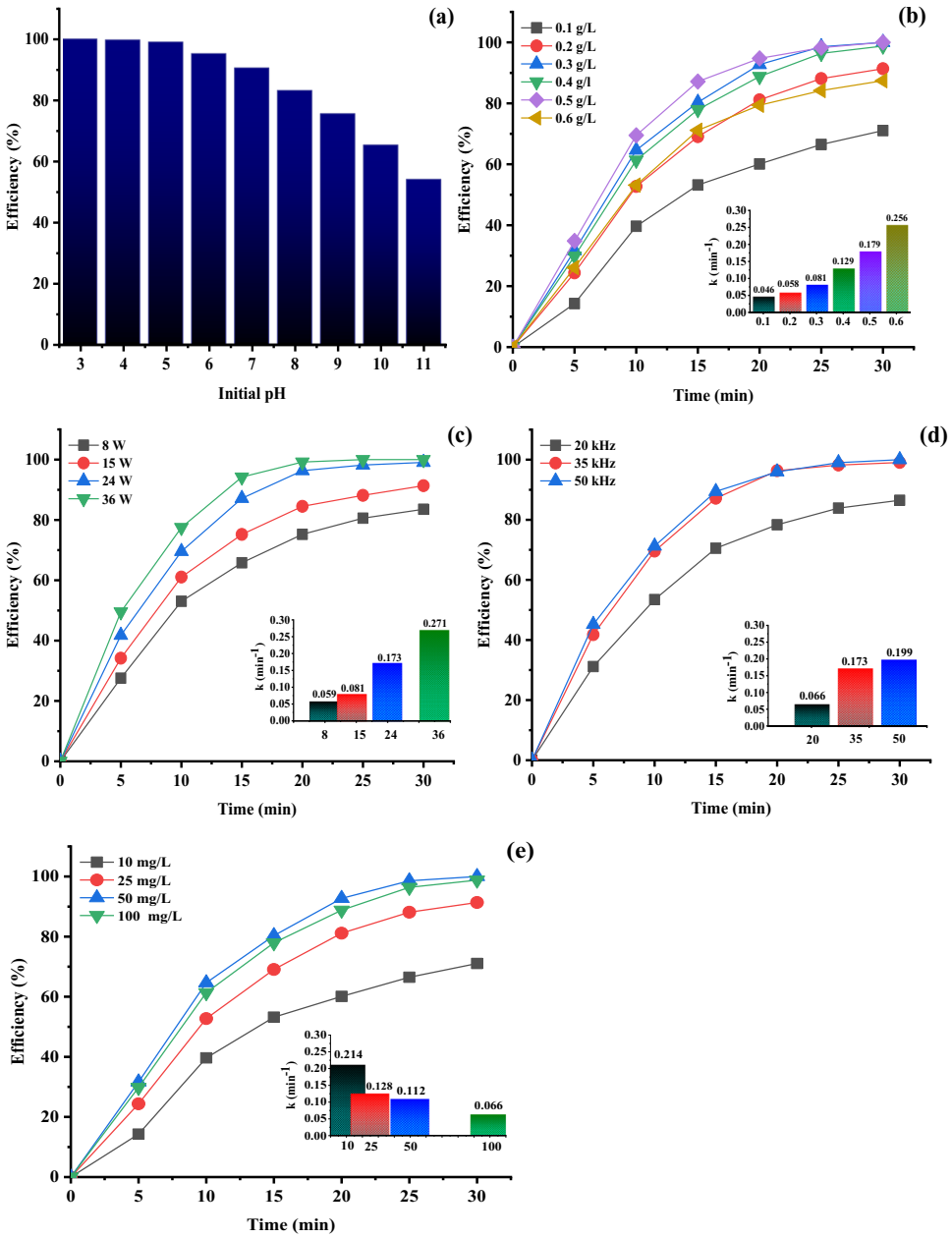

Fig. 4 The effect of pH value (**a**), MWCNT–$CuNiFe_2O_4$ dosage (**b**), UV light intensity (**c**), US frequency (**d**), and initial AB113 dye concentration (**d**) on the photocatalytic degradation efficiency of the AB113 dye

in Fig. 4b (conditions: pH = 5, dye concentration = 50 mg/L, ultrasound frequency = 35 kHz, and UV intensity = 36 W).

The degradation efficiency of the AB113 dye increases from 73.96 to 100%, with an increase in the photocatalyst dose from 0.1 to 0.6 g/L. Also, the pseudo-first-order (PFO) model has been applied in this research to study the kinetic reaction of the AB113 dye degradation. In fact, this model is greatly linked to the degradation reactions of organic pollutants using the advanced oxidation process, expressed as Eq. (2) (Kamranifar et al., 2021). On the basis of the PFO model, and evident from Fig. 4b, the data of $\ln \frac{C_0}{C_e}$ is plotted against the reaction time (t, min), seen as a straight line, while the slope of the graph reveals the rate constant (k, min^{-1}).

$$\ln \frac{C_0}{C_e} = kt \tag{2}$$

From the kinetic analysis, the constant rate of kinetics improved from 0.046 to 0.256 min^{-1} by increasing the MWCNT–$CuNiFe_2O_4$ dosage. This may relate to an increase in the specific surface area of the photocatalyst to adsorb pollutants and photons. In addition, the presence of more active sites increases the production rate of cavitation bubbles, which produce more reactive species for

photodegradation. These results were similar to the findings of Rad et al. for sonophotocatalytic degradation of the AB113 dye by FeCuMg and CrCuMg (Rad et al. 2020) [37]. Tabasideh et al. also observed a similar behavior in the Fe–TiO_2 dosages for the sonophotocatalytic degradation of diazinon. They reported that the pollutant degradation efficiency was significantly improved by increasing the active surface area and cavitation activity (Tabasideh et al. 2017).

The effect of the applied intensity of UV light on the AB113 dye degradation efficiency under operating conditions, including a pH of 5, MWCNT–$CuNiFe_2O_4$ dosage of 0.6 g/L, dye concentration of 50 mg/L, and an ultrasound frequency of 35 kHz, was presented in Fig. 4c. It was noted that by increasing UV intensity from 8 to 36 W, AB113 degradation efficiency increased significantly from 80.59 to 100% at a reaction time of 25 min. The results of the kinetic analysis showed a similar trend. The constant kinetic rates obtained for the intensities of 8, 15, 24, and 36 W were 0.059, 0.081, 0173, and 0.275 min^{-1}, respectively. This increase of efficiency may be caused by the development of free radicals through the abundance of excited e^-/h^+ pairs. During this abundance, the reaction rate between the dye molecules and the active sites increases and the possibility of dye oxidation improves. This may also result from the enhancement production of reactive species through water molecule hydrolysis by UV alone. A similar result was reported by Mamun Reza et al. for photocatalytic analysis. They explained that efficiency improvement was caused by the production of more protons needed to transfer electrons from a valence band level to the conduction band level to produce more reactive species (Reza et al. 2017).

Figure 4d shows the effect of US frequency (20, 35, and 50 kHz) on dye degradation (conditions: pH = 5, dye concentration = 50 mg/L, MWCNT–$CuNiFe_2O_4$ dosage of 0.6 g/L, and UV intensity = 36 W). As expected, by increasing the frequency from 20 to 35 kHz, the degradation efficiency increased from 86.49 to 99.06%, at a reaction time of 30 min. In addition, the results of the kinetic analysis showed that the constant rate values had increased from 0.066 to 0.173 min^{-1} with the same increase in ultrasonic frequency. This could have been caused by the increase in cavitation flow, to develop a mass transfer rate in the aqueous phase and the release rate of reactive species. The surface of MWCNTs–$CuNiFe_2O_4$ could be cleaned more, under high ultrasound waves, which might increase the catalytic activity of the photocatalyst (Wang et al. 2008). In other words, in the sonophotocatalytic process, the production of hydroxyl radicals and the formation of holes on the surface or the inner catalyst depended on cavitation. In addition, with increasing the frequency, the adsorption ability of nanoparticles decreased with increasing temperature (which was caused by increasing the frequency), which caused a large number of contaminant molecules to escape from the active sites of the catalyst and lose the chance of decomposition. However, with a further increase in frequency to 50 kHz, the efficiency and kinetic rate did not change significantly. Thus, the frequency of the ultrasound waves was fixed at 35 kHz for the subsequent experiments. Such results agree with the findings of Kumar et al. and He et al. (2011), for the degradation of methylene orange. They explained that the improvement in efficiency at high frequencies was caused by the synergistic effect of sonolysis and photolysis on the production of more •OH (Eqs. (3), (4) and (5)).

$$H_2O +))))^{US} \rightarrow {}^{\cdot}OH + {}^{\cdot}H \tag{3}$$

$${}^{\cdot}OH + {}^{\cdot}H \rightarrow H_2O_2 \tag{4}$$

$$H_2O_2 + UV \rightarrow {}^{\cdot}OH + {}^{\cdot}H \tag{5}$$

The effect of different concentrations of the AB113 dye on its degradation efficiency has been investigated at pH of 5, MWCNT–$CuNiFe_2O_4$ dosage of 0.6 g/L, UV intensity of 36 W, and ultrasound frequency of 35 kHz. The results are presented in Fig. 4e, which reveal that low dye concentrations have both higher degradation efficiencies and constant kinetic rates as compared to other dye concentrations. This decrease in efficiency at high concentrations of the AB113 dye can be explained as follows: in the presence of constant values of the photocatalyst dose, UV intensity, and ultrasonic frequency, a constant amount of the e^-/h^+ pair is produced for the degradation of the contaminant. High concentrations of the AB113 dye molecules will hamper the photon adsorption rate on the surface of the used catalyst during photocatalytic reactions. This phenomenon will lead to a reduction in the production of radicals and thus reduce the degradation of pollutants. A similar behavior was observed by the photocatalyst used in previous studies (Wang et al. 2008; Vigneshwaran et al. 2020; Balarak et al. 2019).

Catalyst activity indifferent treatment systems

Figure 5a shows a comparison of the adsorption, photolysis, sonolysis, sonocatalytic, photocatalytic, and sonophotocatalytic processes in the removal of AB113 under operating conditions including a pH of 5, ultrasonic frequency of 35 kHz, UV intensity of 24 W, and a catalyst dose of 0.6 g/L. As can be seen, sonolysis and photolysis, at a reaction time of 30 min, have degradation efficiencies of 35.94% and 23.34%, respectively. These results emphasize that the present processes can reliably degrade the AB113 dye into products, by breaking down water molecules into reactive species besides leaving a direct effect on the pollutant molecules. The dye removal efficiency was significantly improved by the adsorption process, with an increase in time, so the

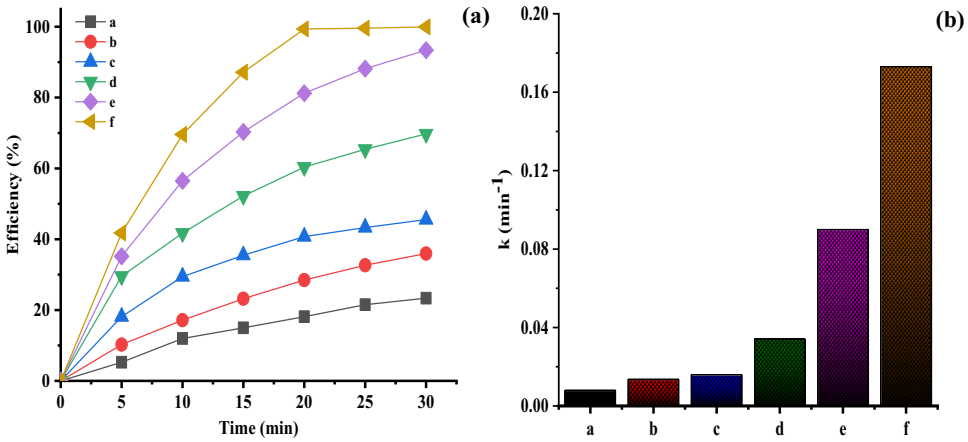

Fig. 5 Values of AB113 dye removal efficiencies (**a**) and kinetic rate (**b**) using different processes, where a, b, c, d, e, and f letters denote photolysis, sonolysis, adsorption, sonocatalytic, photocatalytic, and sonophotocatalytic processes, respectively

maximum removal efficiency became 45.56% in 30 min. This increase might be caused by the point of zero charge property of the catalyst (PZC = 7.8) and by the dissociation constant of the dye (pKa = 0.5). Based on these properties, at a pH of 5, strong adsorption can occur between the dye molecules and functional groups of MWCNTs–$CuNiFe_2O_4$. When the catalyst is added to the photolysis and sonolysis reactors, the degradation efficiency increases significantly from 69.73 to 93.39%. This increase in sonocatalysis may result from the ultrasonic effect on the refreshed surface of the catalyst and better dispersion of the catalyst in the reactor. In addition, the ultrasound can break down water molecules to produce free radicals by creating cavitation bubbles. In a photocatalysis reactor, energy photons are absorbed on the surface of the catalyst, and the electron is excited in the valence band to the conduction band, to produce h^+. Holes decompose the water molecules to produce more •OH. These results agree with the studies on sonocatalytic (Fatimah et al. 2020) and photocatalytic (Asgari et al. 2020) degradation of organic pollutants. Compared to the above processes, the sonophotocatalytic process (US/UV/MWCNTs–$CuNiFe_2O_4$) provides a complete degradation of the dye at a reaction time of 20 min. This high rate of degradation may have resulted from the increasing production of •OH during the synergistic effect of the processes mentioned above. To confirm the synergistic effect of the sonolysis and photocatalysis processes, the first-order kinetic constant rate calculations were performed (Fig. 5b); then the synergy rate of the process was evaluated with Eq. (6). Such results showed that the sonophotocatalytic degradation system has a 1.4 fold to the synergistic effect. These high amounts of removal may be referred back to the effect of the ultrasound on H_2O_2 production and its decomposition by UV light to produce •OH. Ultrasound waves, in the reactor, also improve the collision of particles with the pollutant in the adsorption–desorption process. Similar results for the degradation of organic pollutants by Fe–TiO_2 were also reported by Tabasideh et al. (Tabasideh et al. 2017).

$$Synergy = \frac{k(sonophotocatalytic)}{k(sonocatalytic + photocatalytic)} \quad (6)$$

To better evaluate the performance of MWCNTs–$CuNiFe_2O_4$, a comparison of sonophotocatalytic efficiency of the catalysts in the removal of organic pollutants is shown in Table 1. As can be seen, the removal efficiency varies between 90 and 100%, which is probably due to differences in the structural properties of the particles in the catalyst used, operating conditions, and properties of the contaminant. $CuNiFe_2O_4$ loaded on MWCNTs in the present study showed an excellent efficiency of AB113 degradation, which could possibly be related to the synergistic effects of Fe_2O_4 on the rapid electron transfer, to produce $O_2^{\bullet-}$, in addition to the acceleration of participation of h^+ in •OH production. Moreover, the results in Table 1 also show that the sonophotocatalytic process using MWCNTs–$CuNiFe_2O_4$ has a high removal efficiency during the short reaction time, when compared to other MWCNTs and UV-based processes. This may be due to the beneficial effect of ultrasound on the photocatalytic process. According to previous studies (Wang et al. 2008; Rajiv et al. 2021), the effect of the ultrasound can be caused by the following reasons: (1) the ultrasound can produce more reactive species through the breakdown of water molecules; (2) cavitation can improve mass transfer between the aqueous phase and photocatalyst surface and can also increase the dispersion of particles for catalytic activity; (3) acoustic cavitation can clean the surface of the photocatalyst and also regenerate the active catalyst sites during the process (Ouyang and Xie 2013).

Identification of oxidative radicals

To investigate the reactive or radical species responsible for the sonophotocatalytic degradation of AB113 via MWCNTs–$CuNiFe_2O_4$, trapping experiments were performed with various scavengers such as EDTA, IPA, and BQ. The results in Fig. 6a show that the degradation efficiency was

Table 1 Comparison of MWCNT–$CuNiFe_2O_4$/UV/US system performance with other similar oxidation processes

Oxidation systems	Operational conditions	Efficiency (%)	Reference
ZnO–GAC/PS/US	Catalyst = 0.5 g/L, dye = 0.5 g/L, US = 60 W, and pH = 3	91.2	(Liu et al. 2018)
ZnO/UV/US	Catalyst = 2 g/L, dye = 50 mg/L, US = 95 W, pH = 2.5, and UV = 4.4 mW/cm^2	100	(Ertugay and Acar 2014)
ZnO/PS/UV/US	Catalyst = 0.5 g/L, dye = 2.5 mg/L, US = 1 W/cm^2, pH = 5.8, and time = 25 min	98.7	(Asgari et al. 2020)
MWCNTs/TiO_2/CdS	MWCNTs/TiO_2/CdS = 1.2 g/L, dye = 20 mg/L, pH = 2.6, and time = 90 min	100	(Ouyang and Xie 2013)
N–Cu co-doped TiO2@CNT/UV/US	Catalyst = 0.8 g/L, pollutant = 60 mg/L, UV = 200 W, pH = 6, US = 200 W, and time = 60 min	100	(Isari et al. 2020)
CeO2–ZrO_2@MOS_2	Catalyst = 0.5 g/L, pH = 5.8, and time = 40 min	96	(Talukdar et al. 2021)
$FeVO_4$@CeO_2/UV/US	Catalyst = 0.1 g/L, pollutant = 20 mg/L, pH = 7, US = 160 W, and time = 30 min	100	(Eshaq and ElMetwally 2020)
Bmim[OAc]-Cu_2O/g-C_3N_4/UV/US	Catalyst = 0.1 g/L, pollutant = 20 mg/L, pH = 7, UV = 6 W, US = 20 kHz, and time = 30 min	100	(Eshaq et al. 2019)
MWCNTs–$NiFe_2O_4$/UV	Time = 300 min	90≈	(Zhu et al. 2015)
$NiFe_2O_4$/MWCNTs/ZnO/UV	Catalyst = 1 g/L, pollutant = 20 mg/L, pH = 11.55, and time = 300 min	95≈	(Hezam et al. 2020)
$CuBi_2O_4$/MWCN/UV	Catalyst = 1 g/L, pollutant = 10 mg/L, and time = 120 min	90≈	(Chen et al. 2016)
MWCNTs–$CuNiFe_2O_4$/UV/US	Catalyst = 0.5 g/L, pollutant = 50 mg/L, pH = 5, UV = 36 W, US = 35 kHz, and time = 30 min	100	This study

decreased in the presence of all these three scavengers, indicating that all free radical species were responsible for dye degradation. Specifically, by adding EDTA to the reaction solution, the degradation efficiency was significantly reduced from 100% in the reactor, without a scavenger to 69%, indicating that h^+ was the major reactive species in the AB113 degradation process. Contrary to that, IPA presence in the reactor reduced the efficiency from 100 to 78%. These results emphasized that •OH, like h^+, was a reactive species responsible for photocatalytic degradation. Adding BQ caused a relatively small reduction in the degradation efficiency, indicating a low effect of $O_2^{\bullet-}$ on the degradation of AB113 in the sonophotocatalytic reactor.

Based on the results above and from the previous studies (Hezam et al. 2020; Asgari et al. 2020).[34, 43], the mechanism of sonophotocatalytic degradation of AB113 was proposed according to Fig. 7. Initially, the AB113 dye molecules were adsorbed on the outer surface of the MWCNT–$CuNiFe_2O_4$ particles. By UV light radiation, the electrons (e-) in the valence band level of the $CuNiFe_2O_4$ surface were excited to the conduction band level, and holes (h^+) were formed in the valence band of the $CuNiFe_2O_4$ particles. The generated electron was transferred to the MWCNT surface to reduce the recombination of e^-/h^+, to produce $O_2^{\bullet-}$ from the dissolved O_2 in the solution. Holes decomposed water molecules to produce •OH. Ultrasonic radiation in the reaction reactor could form microbubbles and decompose water to form oxidative species (•OH and $O_2^{\bullet-}$). On the other hand, ultrasonic waves coupled with the catalyst could improve the production of the e^-/h^+ pairs by providing energy. Finally, the produced reactive species such as h^+, •OH, and $O_2^{\bullet-}$ could decompose the surface-adsorbed AB113 molecules into simple compounds like carbon dioxide (CO_2), water (H_2O), and other byproducts. All mechanisms could be demonstrated by the following reactions (Eqs. (7), (8), (9), (10), (11) and (12)):

$$MWCNTs - CuNiFe_2O_4 + hv \rightarrow MWCNTs - CuNiFe_2O_4(e^-_{CB} + h^+_{VB}) \quad (7)$$

$$MWCNTs - CuNiFe_2O_4 + ultrasound))) \rightarrow MWCNTs - CuNiFe_2O_4(e^-_{CB} + h^+_{VB}) \quad (8)$$

$$e^-_{CB} + O_2 \rightarrow O_2^{-\cdot} \quad (9)$$

$$h^+_{VB} + H_2O \rightarrow \cdot OH + H^+ \quad (10)$$

$$Ultrasound))) + H_2O \rightarrow \cdot OH + H^+ \quad (11)$$

$$\cdot OH/h^+_{VB}/\cdot O_2^- + AB113 \rightarrow CO_2 + H_2O + degradable\ by\ products \quad (12)$$

Reusability and stability of the catalyst

Proper stability is one of the important parameters in the actual application of the catalysts in the sonophotocatalytic process. In this study, the reusability of MWCNTs–$CuNiFe_2O_4$ was investigated in eight consecutive reaction cycles (pH of 5, catalyst dosage of 0.8 g/L, AB113

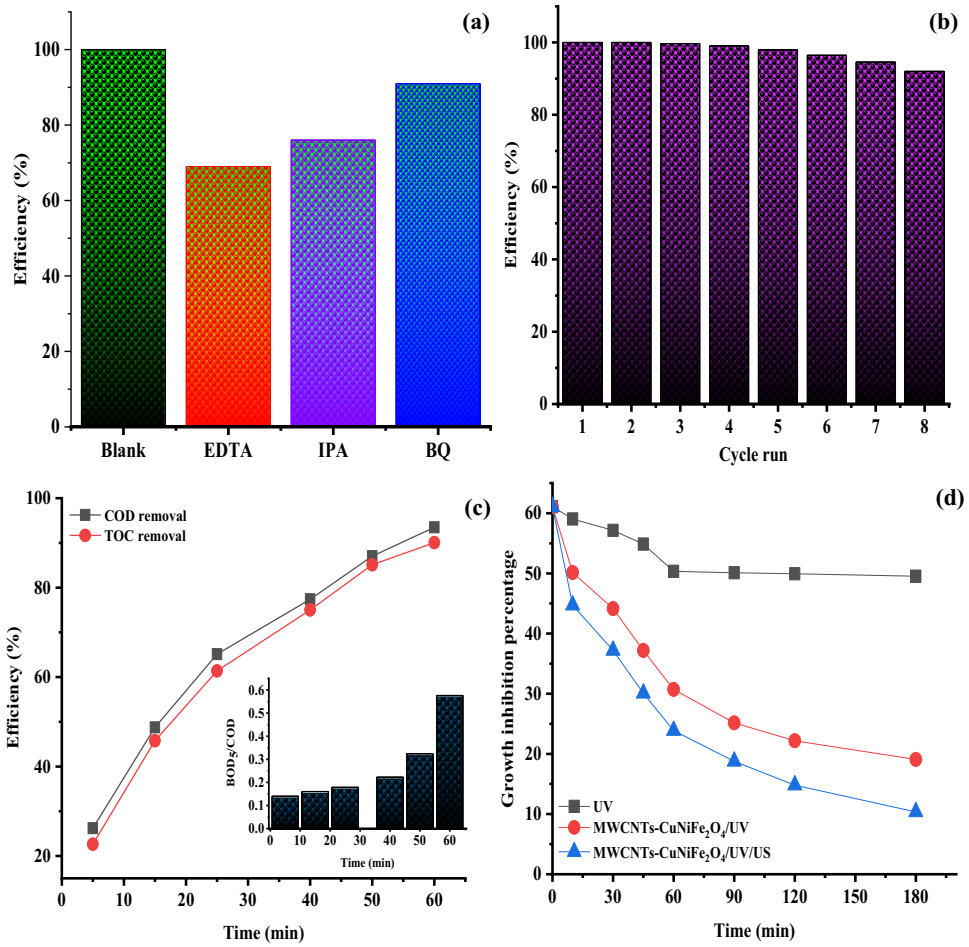

Fig. 6 Effect of various scavengers on the degradation efficiency of the AB113 dye (**a**), photocatalyst reusability experiments (**b**), COD and TOC removal efficiency (inset figure indicates of BOD_5/COD rate) (**c**), and toxicity evaluation of the treated AB113 dye solution (**d**)

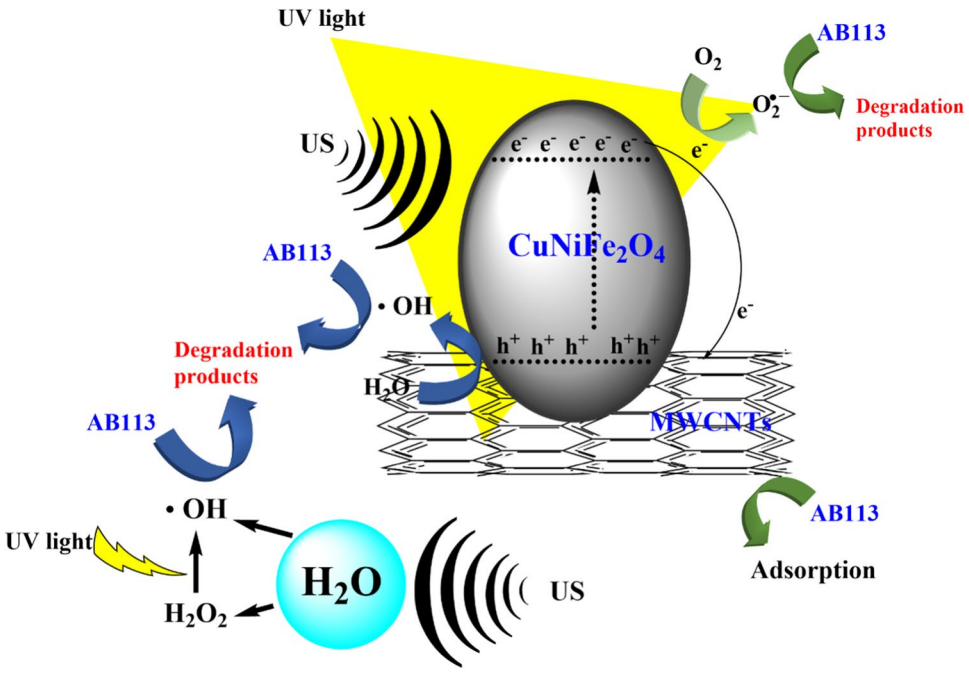

Fig. 7 Schematic illustration of the proposed mechanism for MWCNT–$CuNiFe_2O_4$/UV/US system

concentration of 50 mg/L, US frequency of 35 kHz, UV intensity of 36 W, and reaction time of 30 min). This can be seen in Fig. 6b through the increasing reaction cycle from 1 to 8. The degradation efficiency decreases relatively slightly, from 100 to 92.02%. This decrease in efficiency may be caused by the loss of some catalysts during the reuse process and the saturation of some active catalyst sites. However, the reusability for eight cycles, with an efficiency of over 92%, shows that the new MWCNT–$CuNiFe_2O_4$ nanocomposite can be used for effective degradation in the sonophotocatalytic system. Hezam et al. revealed a high reusability potential of MWCNTs/$NiFe_2O_4$/ZnO. They found that the photocatalyst structure that was based on MWCNTs remained unchanged after five consecutive reaction cycles (Balarak et al. 2021).

Mineralization and toxicity studies

Since the provision of a treatment solution with excellent and nontoxic mineralization is one of the main objectives of the wastewater treatment process, a number of experimental runs were performed to investigate the mineralization and biodegradability of the effluent. Figure 6c shows the removal efficiency of TOC and COD in the MWCNT-$CuNiFe_2O_4$/US/UV reactor. A significant increase in the COD (93.49%) and TOC (90.06%) removal efficiencies were observed in a reaction time of 30 min. During this reaction time, the COD and TOC concentrations decreased from 359.5 and 41.72 mg/L to 23.4 and 4.146 mg/L, respectively. This indicates that a short reaction time is needed for AB113 dye mineralization. In addition, the significant efficiency of the sonophotocatalytic process using MWCNTs–$CuNiFe_2O_4$ in AB113 dye mineralization can be related to the high adsorption rate and the excellent performance of the e^-/h^+ pair in increasing the production of active radicals. Similar results were also reported by Asgari et al. regarding the mineralization of AB113 by US/UV/ZnO/PS (Asgari et al. 2020). The inset of Fig. 6c shows that the BOD_5/COD ratio represents changes in the biodegradability of the AB113 solution, during the sonophotocatalytic process. It could be noted that by increasing the reaction time from 5 to 30 min, the BOD_5/COD ratio significantly improved from 0.13 to 0.57. These results indicate that the present process can reduce the toxicity of the solution and can increase the biodegradability of the mixture.

To confirm the above results, toxicity changes during direct photolysis, photocatalysis, and sonophotocatalytic processes were investigated based on the growth inhibition percentage of *E. coli* (Eq. 13). As shown in Fig. 6d, a gentle decrease in bacterial growth inhibition was observed by increasing the time from zero to 180 min, during direct photolysis. This reduction was 11.55% in reaction time, between zero and 180 min. Small changes in growth inhibition indicated that a high ratio of toxic products were produced during the photolysis reaction. By adding MWCNTs–$CuNiFe_2O_4$ to the photolysis reactor, the inhibition rate significantly reduced from 61.08 to 19.08%. These results were confirmed by the high removal rates of the AB113 dye (100%) and TOC (90%). Compared to the above processes, the sonophotocatalytic process reduced the inhibition percentage from 61.08 to 10.35%. Such results suggested that the present degradation process could be proposed as a pretreatment process before the biological treatment to facilitate the degradation of stable compounds.

$$Growth\ inhibition\ percentage = \left(1 - \frac{OD_{600S}}{OD_{600B}}\right) \times 100 \quad (13)$$

where OD_{600S} and OD_{600B} are the optical density of sample and control at 600 nm, respectively.

Identification and change of inorganic ions

Mineralization of a pollutant with carbon, sulfur, and nitrogen atoms produces CO_2, SO_4^{2-}, and nitrogenous compounds (such as NH_4^+ and NO_3^-). To specify the degree of mineralization of the AB113 dye, the concentrations of NH_4^+, NO_3^-, and SO_4^{2-} released during the sonophotocatalytic process were measured, and the results are shown in Fig. 8. The concentration of NH_4^+ ions formed during AB113 dye mineralization increased from 0.29 to 2.58 mg/L over 10 to 120 min. In contrast, the concentration of NO_3^- at the initial time is zero; then by increasing the treatment time to 120 min, the concentration reaches 1.64 mg/L. These results indicate that most of the nitrogen is likely to be combined with intermediates or is lost as nitrogen gases (Wakrim et al. 2021). The concentration of SO_4^{2-} in Fig. 8 increases from zero to 1.84 mg/L in 120 min. These results

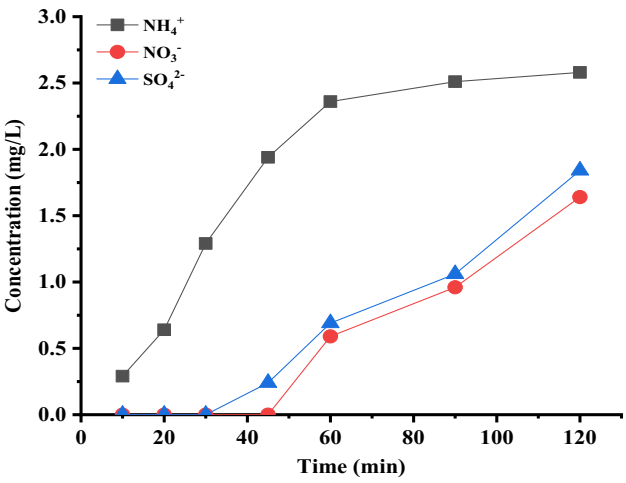

Fig. 8 Concentrations of NH_4^+, NO_3^-, and SO_4^{2-} ions detected during 120 min of the sonophotocatalytic degradation of the AB113 dye

also emphasize that most of the – SO_3^-group remains in the structure of AB113 at the early stages of oxidation in the byproducts and then slowly transforms into SO_4^{2-} ions.

Conclusion

The MWCNT–$CuNiFe_2O_4$ nanocomposite was synthesized for use as an efficient catalyst in the effective sonophotocatalytic degradation of the AB113 dye. Based on the findings of the present study, the mixed ferrite nanoparticles on MWCNTs showed a high degradation activity and stability in the sonophotocatalytic reactor. The complete AB113 degradation in the MWCNT–$CuNiFe_2O_4$/UV/US system may be caused by the participation of the produced reactive species such as $O_2^{\bullet-}$, h^+, and •OH. Photocatalyst stability showed that MWCNTs–$CuNiFe_2O_4$ can be recycled for eight consecutive reaction cycles, with minimal reduction of efficiency. The study of mineralization and biodegradability of the synthetic solution was performed by determining the removal rates of TOC, COD, and BOD_5/COD. The results showed a 93 to 95% reduction for COD and TOC, at a reaction time of 30 min. Changes in the BOD_5/COD rate from 0.13 to 0.57, with increasing time of degradation from 5 to 30 min, confirmed that the present process could be used as a biological pretreatment system. The analysis of the toxicity and concentration of inorganic ions (such as NH_4^+, NO_3^-, and SO_4^{2-}) in the treated solution emphasized that the sonophotocatalytic process using MWCNTs–$CuNiFe_2O$ was an effective and promising treatment method for dye degradation in aqueous solutions.

Acknowledgements The authors are grateful to the Zahedan University of Medical Sciences (Iran) and Al-Mustaqbal University College (Iraq).

Author contribution All authors contributed to the study conception and design. Material preparation, data collection, and analysis were performed by Tariq J. Al-Musawi, Nezamaddin Mengelizadeh, Mahmoud Taghavi, and Zaccheus Shehu. The first draft of the manuscript was written by Davoud Balarak. All authors commented on the previous versions of the manuscript. All authors read and approved the final version of the manuscript.

Funding This study was supported by the Zahedan University of Medical Sciences, Zahedan-Iran. (Code:10528).

Data availability The datasets used and analyzed during the current study are available from the corresponding author on reasonable request.

Declarations

Ethics approval Not applicable.

Consent for participate Not applicable.

Consent for publication Not applicable.

Competing interests The authors declare no competing interests.

References

Alhassani MH, Al-Jubouri SM, Al-Jendeel HA (2020) Stabilization of phenol trapped by agricultural waste: a study of the influence of ambient temperature on the adsorbed phenol. Desalin Water Treat 2020(187):266–276

Al-Jubouri SM, Al-Batty SI, Senthilnathan S, Sihanonth N, Sanglura L (2021) Utilizing Faujasite-type zeolites prepared from waste aluminium foil for competitive ion-exchange to remove heavy metals from simulated wastewater. Desalin Water Treat 231:166–181

Al-Musawi TJ, Rajiv P, Mengelizadeh N, Arghavan FS (2021) Photocatalytic efficiency of CuNiFe2O4 nanoparticles loaded on multi-walled carbon nanotubes as a novel photocatalyst for ampicillin degradation. J Mol Liq 337

Al-Musawi TJ, Rajiv P, Mengelizadeh N, Mohammed IA, Balarak D (2021) Development of sonophotocatalytic process for degradation of acid orange 7 dye by using titanium dioxide nanoparticles/graphene oxide nanocomposite as a catalyst. J Environ Manage 292

Amiri M, Eskandari K, Salavati-Niasari M (2019) Magnetically retrievable ferrite nanoparticles in the catalysis application. Adv. Colloid Interface Sci 271

Asgari G, Shabanloo A, Salari M, Eslami F (2020) Sonophotocatalytic treatment of AB113 dye and real textile wastewater using ZnO/persulfate: modeling by response surface methodology and artificial neural network. Environ Res 184

Asghar A, Bello MM, Raman AA (2019) Predicting the degradation potential of acid blue 113 by different oxidants using quantum chemical analysis. Heliyon 5:392–396

Babu SG, Aparna P, Satishkumar G, Ashokkumar M, Neppolian B (2017) Ultrasound-assisted mineralization of organic contaminants using a recyclable $LaFeO_3$ and Fe^{3+}/persulfate Fenton-like system. Ultrason Sonochem 34:924–930

Babu SG, Karthik P, John MC, Lakhera SK, Ashokkumar M, Khim J, Neppolian B (2019) Synergistic effect of sono-photocatalytic process for the degradation of organic pollutants using CuO-TiO2/rGO. Ultrason Sonochem 50:218–223

Balarak D, Mengelizadeh N, Rajiv P (2021) Photocatalytic degradation of amoxicillin from aqueous solutions by titanium dioxide nanoparticles loaded on graphene oxide. Environ Sci Pollut Res Int. https://doi.org/10.1007/s11356-021-13525-1

Balarak D, Mostafapour FK (2019) Photocatalytic degradation of amoxicillin using UV/synthesized NiO from pharmaceutical wastewater. Indones J Chem 19(1):211–218

Bolong N, Ismail A, Salim MR, Matsuura T (2009) A review of the effects of emerging contaminants in wastewater and options for their removal. Desalination 239:229–246

Chahar D, Taneja S, Bisht S, Kesarwani S, Thakur P, Thakur A, Sharma P (2021) Photocatalytic activity of cobalt substituted zinc ferrite for the degradation of methylene blue dye under visible light irradiation. J Alloys Compd 851

Cheng Z, Quan Y, Xiong L, Yang Y (2012) Synergistic degradation of methyl orange in an ultrasound intensified photocatalytic reactor. Ultrason Sonochem 19:1027–1033

Chen M, Yang Q, Li L, Liu M, Xiao P, Zhang M (2016) Solid-state synthesis of $CuBi_2O_4$/MWCNT composites with enhanced photocatalytic activity under visible light irradiation. Mater Lett 171:255–258

Dojcinovic MP, Vasiljevic ZZ, Pavlovic VP, Barisic D, Pajic D, Tadic NB, Nikolic MV (2021) Mixed Mg–Co spinel ferrites:

structure, morphology, magnetic and photocatalytic properties. J Alloys Compd 855
Ertugay N, Acar FN (2014) The degradation of Direct Blue 71 by sono, photo and sonophotocatalytic oxidation in the presence of ZnO nanocatalyst. Appl Surf Sci 318:121–126
Eshaq G, Wang S, Sun H, Sillanpaa M (2020) Superior performance of FeVO4@CeO2 uniform core-shell nanostructures in heterogeneous Fenton-sonophotocatalytic degradation of 4-nitrophenol. J Hazard Mater 382
Eshaq G, ElMetwally AE (2019) Bmim [OAc]-Cu_2O/g-C_3N_4 as a multi-function catalyst for sonophotocatalytic degradation of methylene blue. Ultrason Sonochem 53:99–109
Fatimah I, Nurillahi R, Sahroni I, Fadillah G, Nugroho B. H, Kamari A, Muraza O (2020) Sonocatalytic degradation of rhodamine B using tin oxide/montmorillonite. J Water Process Eng 37:101418
Federation WE, Association A (2005) Standard methods for the examination of water and wastewater, American Public Health Association (APHA): Washington. DC, USA
Hanh NT, Van D, Thuan NM, Khai PT (2020) Synthesis of Co_3O_4 coated on N, S doped TiO_2 for novel photocatalytic degradation of toxic organic pollutant in aqueous environment. Ceram Int 46:21610–21616
He Y, Grieser F, Ashokkumar M (2011) The mechanism of sonophotocatalytic degradation of methyl orange and its products in aqueous solutions. Ultrason Sonochem 18:974–980
Hezam F, Nur O, Mustafa M (2020) Synthesis, structural, optical and magnetic properties of NiFe2O4/MWCNTs/ZnO hybrid nanocomposite for solar radiation driven photocatalytic degradation and magnetic separation. Colloids Surf A 592
Isari AA, Hayati F, Kakavandi B, Rostami M, Motevassel M, Dehghanifard E (2020) N, Cu co-doped TiO_2@ functionalized SWCNT photocatalyst coupled with ultrasound and visible-light: an effective sono-photocatalysis process for pharmaceutical wastewaters treatment. Chem Eng J 392:123685
Ji H, Jing X, Xu Y, Yan J, Li H, Y. Y, Huang L, (2015) Magnetic g-C_3N_4/$NiFe_2O_4$ hybrids with enhanced photocatalytic activity. RSC Adv 5:57960–57967
Kamranifar M, Al-Musawi TJ, Amarzadeh M, Qutob M, Arghavan FS (2021) Quick adsorption followed by lengthy photodegradation using $FeNi_3$@SiO_2@ZnO: a promising method for complete removal of penicillin G from wastewater. J Water Process Eng 40:101940
Liu F, Yi P, Wang X, Gao H, Zhang H (2018) Degradation of acid Orange 7 by an ultrasound/ZnO-GAC/persulfate process. Sep Purif Technol 194:181–187
Liu T, Qian J, Wang C, Wang Y, Yang Y, Kong B, Qian Y, Wu W, (2020) Enhanced photocatalytic degradation performance of mono-disperse ZnS nano-flake on biocarbon sheets. Inorg Chem Commun 119:108142
Manohar A, Chintagumpala K, Kim KH (2021) Mixed Zn–Ni spinel ferrites: structure, magnetic hyperthermia and photocatalytic properties. Ceram Int 47:7052–7061
Meena S, Anantharaju K, Vidya Y, Renuka L, Uma B, Sharma S, More SS (2021) Enhanced sunlight driven photocatalytic activity and electrochemical sensing properties of Ce-doped $MnFe_2O_4$ nano magnetic ferrites. Ceram Int 47:14760–14774
Moazzen M, Khaneghah AM, Shariatifar N, Ahmadloo M, Baghani AN, Yousefinejad S (2019) Multi-walled carbon nanotubes modified with iron oxide and silver nanoparticles (MWCNT-Fe_3O_4/Ag) as a novel adsorbent for determining PAEs in carbonated soft drinks using magnetic SPE-GC/MS method. Arabian J Chem 12:476–488
Mortazavian S, Saber A, James DE (2019) Optimization of photocatalytic degradation of acid blue 113 and acid red 88 textile dyes in a UV-C/TiO_2 suspension system: application of response surface methodology (RSM). J Catalysts 9:360
Muhambihai P, Rama V, Subramaniam P (2020) Photocatalytic degradation of aniline blue, brilliant green and direct red 80 using NiO/CuO, CuO/ZnO and ZnO/NiO nanocomposites. Environ Nanotechnol Monit Manage 14:100360
Mujahid M, Khan RU, Mumtaz M, Soomro SA (2019) $NiFe_2O_4$ nanoparticles/MWCNTs nanohybrid as anode material for lithium-ion battery. Ceram Int 45:8486–8493
Murali A, Sarswat PK, Free ML (2020) Adsorption-coupled reduction mechanism in ZnO-Functionalized MWCNTs nanocomposite for Cr (VI) removal and improved anti-photocorrosion for photocatalytic reduction. J Alloys Compd 843:155835
Natarajan K, Dave S, Bajaj H. C, Tayade RJ (2020) Enhanced photocatalytic degradation of nitrobenzene using MWCNT/β-$ZnMoO_4$ composites under UV light emitting diodes (LEDs). Mater Today Chem 17:100331
Nawaz A, Khan A, Ali N, Bilal M (2020) Fabrication and characterization of new ternary ferrites-chitosan nanocomposite for solar-light driven photocatalytic degradation of a model textile dye. Environ Technol Innovation 20:101079
Ouyang K, Xie S (2013) Effect of key operational factors on decolorization of methyl orange by multi-walled carbon nanotubes (MWCNTs)/TiO_2/CdS composite under simulated solar light irradiation. Ceram Int 39:8035–8042
Rad TS, Ansarian Z, Soltani RD, Khataee A, Orooji Y, Vafaei F (2020) Sonophotocatalytic activities of FeCuMg and CrCuMg LDHs: influencing factors, antibacterial effects, and intermediate determination. J Hazard Mater 399:123062
Rahman A, Warsi MF, Shakir I, Shahid M, Zulfiqar S (2020) Fabrication of Ce^{3+} substituted nickel ferrite-reduced graphene oxide heterojunction with high photocatalytic activity under visible light irradiation. J Hazard Mater 394:122593
Rajabzadeh M, Khalifeh R, Eshghi H, Bakavoli M (2018) A facile hydrothermal synthesis of novel hollow triple-shell $CuNiFe_2O_4$ nanospheres with robust catalytic performance in the Suzuki-Miyaura coupling reaction. J Catalysis 360:261–269
Rajiv P, Mengelizadeh N, McKay G (2021) Photocatalytic degradation of ciprofloxacin with Fe_2O_3 nanoparticles loaded on graphitic carbon nitride: mineralisation, degradation mechanism and toxicity assessment. Int J Environ Anal Chem. https://doi.org/10.1080/03067319.2021.1890059.
Rao P, Godbole R, Bhagwat S (2016) Copper doped nickel ferrite nano-crystalline thin films: a potential gas sensor towards reducing gases. Mater Chem Phys 171:260–266
Reza KM, Kurny A, Gulshan F (2017) Parameters affecting the photocatalytic degradation of dyes using TiO 2: a review. Appl Water Sci 7:1569–1578
Samarghandi MR, Tari K, Shabanloo A, Salari M, Nasab HZ (2020) Synergistic degradation of acid blue 113 dye in a thermally activated persulfate (TAP)/ZnO-GAC oxidation system: degradation pathway and application for real textile wastewater. Sep Purif Technol 247:116931
Schieppati D, Galli F, Peyot ML, Yargeau V, Bianchi C, Boffito D (2019) An ultrasound-assisted photocatalytic treatment to remove an herbicidal pollutant from wastewaters. Ultrason Sonochem 54:302–310
Shabbir A, Ajmal S, Shahid M, Shakir I, Agboola PO, Warsi MF (2019) Zirconium substituted spinel nano-ferrite MgO. 2CaO. 8Fe_2O4 particles and their hybrids with reduced graphene oxide for photocatalytic and other potential applications. Ceram Int 45:16121–16129
Sayadi MH, Ahmadpour N, Homaeigohar S (2021) Photocatalytic and antibacterial properties of Ag-$CuFe_2O_4$@WO_3 magnetic nanocomposite. Nanomater 11:298
Soltani T, Entezari MH (2013) Solar photocatalytic degradation of RB5 by ferrite bismuth nanoparticles synthesized via ultrasound. Ultrason Sonochem 20:1245–1253

Soomro SA, Gul IH, Khan MZ, Naseer H, Khan AN (2017) Dielectric properties evaluation of $NiFe_2O_4$/MWCNTs nanohybrid for microwave applications prepared via novel one step synthesis. Ceram Int 43:4090–4095

Sun J, Feng S (2020) Hydrothermally synthesis of MWCNT/N-TiO_2/UiO-66-NH_2 ternary composite with enhanced photocatalytic performance for ketoprofen. Inorg Chem Commun 111:107669

Tabasideh S, Maleki A, Shahmoradi B, Ghahremani E, McKay G (2017) Sonophotocatalytic degradation of diazinon in aqueous solution using iron-doped TiO_2 nanoparticles. Sep Purif Technol 189:186–192

Talukdar K, Saravanakumar K, Kim Y, Fayyaz A, Kim G, Yoon Y, Park CM (2021) Rational construction of CeO_2–ZrO_2@MoS_2 hybrid nanoflowers for enhanced sonophotocatalytic degradation of naproxen: mechanisms and degradation pathways. Composites, Part B 215:108780

Tan TL, Lee KM, Lai CW, Hong SL, Rashid SA (2020) Photocatalytic degradation mechanisms of dimethyl phthalate esters by MWCNTs-anatase TiO_2 nanocomposites using the UHPLC/Orbitrap/MS technique. Adv Powder Technol 31:533–547

Vigneshwaran S, Jun BM, Prabhu SM, Elanchezhiyan SS, Ok YS, Meenakshi S (2020) Enhanced sonophotocatalytic degradation of bisphenol A using bimetal sulfide-intercalated MXenes, 2D/2D nanocomposite. Sep Purif Technol 250

Yaghoubi A, Nikje MMA (2018) Silanization of multi-walled carbon nanotubes and the study of its effects on the properties of polyurethane rigid foam nanocomposites. Compos A 109:338–344

Wang H, Niu J, Long X, He Y (2008) Sonophotocatalytic degradation of methyl orange by nano-sized Ag/TiO2 particles in aqueous solutions. Ultrason Sonochem 15:386–392

Wakrim A, Dassaa A, Ghachtouli SE, Eddine JJ, Azzi M (2021) Mechanistic study of carmoisine dye degradation in aqueous solution by Fenton process. Mater Today: Proc 37:3847–3853

Zhang X, Feng M, Qu R, Liu H, Wang L, Wang Z (2016) Catalytic degradation of diethyl phthalate in aqueous solution by persulfate activated with nano-scaled magnetic $CuFe_2O_4$/MWCNTs. Chem Eng J 301:1–11

Zhu HY, Jiang R, Huang SH, Yao J, Fu FQ (2015) Novel magnetic NiFe2O4/multi-walled carbon nanotubes hybrids: facile synthesis, characterization, and application to the treatment of dyeing wastewater. Ceram Int 41:11625–11631